water

MDPI

Article

Surface Water Dynamics in the North America Arctic Based on 2000–2016 Landsat Data

Yijie Sui [1,2], Dongjie Fu [1], Xuefeng Wang [3] and Fenzhen Su [1,*]

[1] State Key Laboratory of Resources and Environmental Information System, Institute of Geographic Sciences and Natural Resources Research, CAS, Beijing 100101, China; suiyj.16b@igsnrr.ac.cn (Y.S.); fudongjie@gmail.com (D.F.)
[2] School of Geography, Beijing Normal University, Beijing 100875, China
[3] Faculty of Geomatics, Lanzhou Jiaotong University, Lanzhou 730070, China; wangxf@lreis.ac.cn
* Correspondence: sufz@lreis.ac.cn; Tel.: +86-648-889-56

Received: 8 April 2018; Accepted: 14 June 2018; Published: 22 June 2018

Abstract: At high latitudes, lake and river ecosystems are predominant and these ecosystems are undergoing significant changes due to climate change. Although many scientists have studied lakes and rivers in the Arctic region, the inland water dynamics in this region at the continental scale remain unknown. In this study, the dynamics of the Arctic water were analyzed at the continental scale using Landsat ortho-rectified surface reflectance products of fine spatial and temporal resolutions for the period of 2000–2016, using the random forests method. The results of this study produced the following revelations: (i) the water area is decreasing year by year in the long term; (ii) the water loss and gain always show the same dynamic pattern spatially and temporally; (iii) the spatial distribution of the water budget is strongly linked to permafrost, which implies that permafrost determines the distribution pattern of the water dynamics more than climatic factors; and (iv) the dynamics of the water show a certain rule with surface temperature, but the pattern of the dynamics cannot be explained by temperature alone.

Keywords: Arctic; surface water; dynamics; Landsat; climate change

1. Introduction

In the Arctic region, inland water plays a significant role. Not only does life in the Arctic depend on the water supply from lakes and rivers but, in addition, water influences several other factors such as surface energy balance, the carbon cycle, the habitats of organisms, and soil moisture. Nevertheless, despite the increasing number of studies on Arctic inland water, the distribution and dynamics of inland water in this region remain unclear. Thus, further investigation is required in this area.

Images of satellite sensing have been applied extensively to analyze the changes of surface water in the Arctic from the local scale [1–5]. Smith et al. [3] reported that lakes in Siberia are disappearing. Jones et al. [4] observed an increase in the number of lakes in Alaska. Early in their research, they found a general Arctic water pattern in which lake abundance and surface area appeared to decrease in the discontinuous, sporadic, and isolated permafrost zones while increasing in the continuous permafrost zone [4]. However, the pattern became unclear in additional studies because the research was conducted in a local region. Therefore, it became apparent that the trend needs to be investigated on a regional scale.

Some recent studies used Landsat imagery to map water bodies at a finer spatial resolution [6–10], which can detect water bodies less than 0.01 km^2 and provide more details to characterize the inland water status and dynamics. However, nearly all existing Landsat-derived regional to global inundation

products are extremely limited by the temporal resolution as they were created only once or every ten years [11,12].

Lately, there are some water products [13] using Landsat imagery whose temporal resolution achieved a yearly, even monthly level. Global Surface Water v1.0 [13] shows a series of maps of global inland water from 1984 to 2015 at a monthly resolution. Moreover, Pekel [13] concentrated on global scale analysis and did not analyze the dynamics of the Arctic open water and often overestimated the water (Figure 1). However, the hydrological process and the role of a factor may differ by location, particularly in the Arctic [14], where the special climate and high latitude make the Arctic region unique. So it is important to investigate the pattern of inland water dynamics in the Arctic on a regional scale and at high temporal resolution.

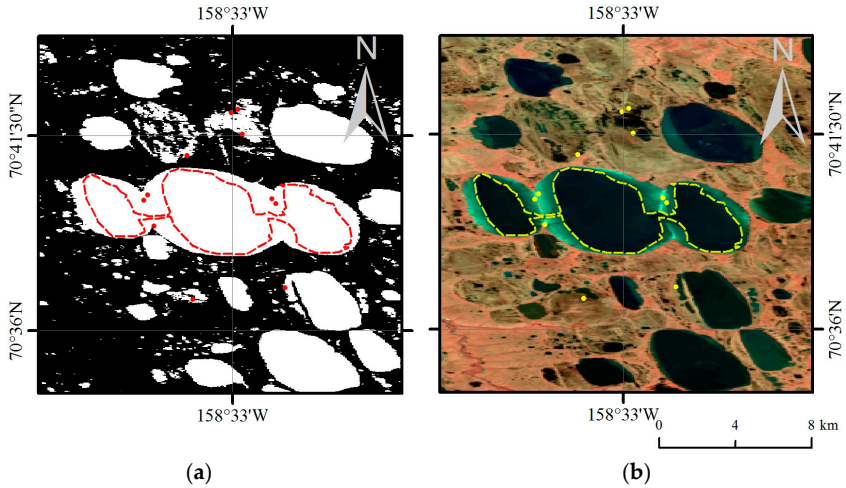

Figure 1. (**a**) The map of Global Surface Water v1.0 (GSW1_0) for 2015. (**b**) The combined Landsat 8 images from April to October in 2015. The red points in (**a**) and the yellow points in (**b**) denote mismatched regions (water in GSW1_0 and land in Landsat).

This present study provides an understanding of the dynamic pattern of inland water in the North American Arctic region (above 60° N) over a 17-year period (2000–2016). In the paper, data from April to October were selected. In addition, the annual inland water dynamics were analyzed.

2. Materials and Methods

2.1. Study Area and Data

The study area includes the Arctic and boreal regions above 60° N in Canada and Alaska. Figure 2 shows the location of the study area.

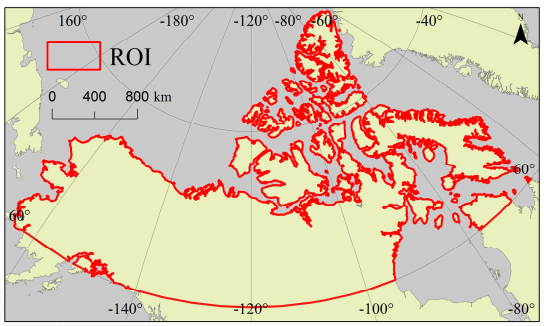

Figure 2. The areas considered within this study (the Arctic and Boreal regions above 60° N in northern North America).

In this paper, Landsat 7 was used to generate data in 2000, both Landsat 5 and 7 were used to generate data from 2001 to 2012, and Landsat 8 was used to generate data from 2013 to 2016. This paper discusses the dynamics of surface water extent during the wet period, thus, all the ice-free data from April to October were selected.

2.2. Methods

We quantified the changes in the Arctic surface water in North America over the past 16 years at a 30-m resolution and used the random forests (RF) supervised classification method to generate the water maps. The Landsat surface reflectance (SR) from April to October for a seventeen-year period between 2000 and 2016 were downloaded from the United States Geological Survey [15]. Using a cloud mask band (CFmask), clouds, cloud shadows, ice, and snow were removed from the scenes. All scenes in the same year were composited by maximizing the normalized difference water index (NDWI) values to observe the water body during the wet season. The ocean mask, terrain shadow mask, and ice mask were applied to the composited images before they were classified.

The cloud shadows, terrain shadows, and glaciers are challenges faced in water detection. Therefore, various indices based on Landsat SR were used to distinguish water from land and other objects. To begin, we used masks to reduce the areas of shadows, seas, and glaciers. The SR product includes the CFmask band, which classifies each pixel as clear, water, cloud, cloud shadow, ice, or snow. The cloud and cloud shadows can be detected by the CFmask band, enabling the use of all the scenes as much as possible.

Terrain shadows are often identified by hill-shade, which is calculated using the parameters of solar azimuth and elevation in a DEM (Digital Elevation Model). Nevertheless, if only the hill-shade is considered, the terrain shadows cannot be identified very accurately, leading to an underestimation of the terrain shadows. The method employed to restrict the thresholds of hill-shade, elevation, and the slope is proven to be effective [14]. In this study, we used the method that restricts the hill-shade, elevation, and slope of DEM to detect water from terrain shadows. Glaciers can be masked by the Randolph Glacier Inventory (RGI 5.0) and seawater can be removed by the MODIS water mask. With the masks, errors cannot be avoided completely; therefore, these images need to be further processed by classification.

Before masking, all the scenes in the same year were composited into an image where each pixel was calculated by the maximum of all the NDWI values in the position of the pixel. Subsequently, we generated water images using the random forests (RF) supervision algorithm. To avoid the inconsistencies in the quality of the local water classification, we selected training points considering all regions where water is present. We used various vegetation and water indices and color parameters to improve the generalization ability of the model. NDWI, MNDWI (Modified Normalized-Difference Water Index), and NDMI (Normalized Difference Moisture Index) were used to distinguish between the water and other objects. NDVI (Normalized Difference Vegetation Index) was used to differentiate the water from the vegetation. The HSV (Hue-Saturation-Value) color model helped to identify the water in the color aspect.

2.3. High-Performance Computing Resources

The Landsat imagery used in this study is available from the Google Earth Engine (https://earthengine.google.com). Google Earth Engine provides online access to all Landsat images and other remote sensing images provided by the United States Geological Survey. This platform makes Landsat data easily accessible to researchers. Furthermore, it allows classification codes to be run on any Landsat 5, 7, and 8 images. In the study, the location of the scenes ranged from 14 to 173, and the row ranged from 1 to 248. A total of 32,927 Landsat scenes were included, with the total data volume exceeding 5.7 TB.

2.4. Indices

Previous studies [9,10,13] have indicated that the NDWI [16], normalized difference vegetation index (NDVI) [17], and normalized difference moisture index (NDMI) [18] can be applied to regional-scale water detection, showing high performance in distinguishing water at different band ranges. The modified normalized-Difference Water Index (MNDWI) [19], which has been widely used to detect water, can differentiate water from soil and buildings. The formulas are as follows:

$$NDWI = (\rho_G - \rho_{NIR})/(\rho_G + \rho_{NIR}) \quad (1)$$

$$MNDWI = (\rho_G - \rho_{SWIR1})/(\rho_G + \rho_{SWIR1}) \quad (2)$$

$$NDMI = (\rho_{NIR} - \rho_{SWIR1})/(\rho_{NIR} + \rho_{SWIR1}) \quad (3)$$

$$NDVI = (\rho_{NIR} - \rho_R)/(\rho_{NIR} + \rho_R) \quad (4)$$

ρ_G is the green band, ρ_{NIP} is the near-infrared band (NIR), ρ_{SWIR1} is the shortwave infrared band (SWIR1), and ρ_R is the red band.

Using a standard transformation, the Hue-Saturation-Value (HSV) and color-space transformations [3] were performed for the following band combinations: shortwave infrared (SWIR1), near-infrared (NIR), red and NIR, green, blue. Recently, the HSV color model has been applied to image identification successfully. This is highly desirable because changes in observation conditions first affect the V component and then the S component, while the H component remains relatively stable (except when the fundamental nature of the target changes, such as when land becomes water). Consequently, this property promotes temporal stability in the measurements and HSV-based classifications have been successfully used for near-real-time surface water detection at continental scales.

2.5. Terrain Mask

We generated a terrain mask with the Global Multi-Resolution Terrain Elevation Data (GMTED) [20], whose best resolution is 250 m. The mask was created by restricting slope and elevation. The slope was calculated from the max rate that the elevation difference was divided by and the distance difference between a pixel and its adjacent pixels. After several experiments, we set the slope to more than 7° and the elevation to more than 1500 m to reduce terrain shadows. This method identifies not only terrain shadows but also the land and parts of the glaciers, which is more effective than using hill-shade.

2.6. Glacier Mask

To avoid interference from glacier shadows, the RGI 5.0 [21] was used to mask the images. The glacier mask removes the areas where glaciers exist, even though it may omit the melted water in such areas.

2.7. Ocean Mask

We removed seawater from the dataset using the MODIS water mask [22]. The MODIS water mask is a global MODIS water mask with a product coverage from 2000 to 2002 and a resolution of 250 m. Firstly, pixels whose elevation (GMTED) was below 5 m and above −5 m were selected from the MODIS water dataset. Then, the analysis converted the selected data to vectors. The largest polygon was detected as the MODIS ocean mask. Next, the Landsat ocean pixels with an elevation below −5 were removed. Then we detected sea regions using the MODIS ocean mask and applied the mask to water maps of this study. Then we buffered the region by 15 pixels to reduce the effect of seawater.

2.8. Classification

Random forests or random decision forests are classifiers containing multiple decision trees, which are combined with "bootstrap aggregating" and the "random subspace method." The introduction of randomness improved the overfitting problem of the decision trees. In addition, this enabled the processing of a large number of input variables, creating a good generalization ability and enhancing robustness. The random forests [23] outlined in the Extended Data Figure 3 were developed to assign each pixel to one of three target classes: water, land, or non-valid observations (snow, ice, cloud, or sensor-related issues). Labels of the training points included two classes: water and land. The numbers of the water and land training points are approximately equal. The selection of water training points considered terrain, the density of water, and the type of water. The land training points were selected from different moisture soil and areas where water was easily classified.

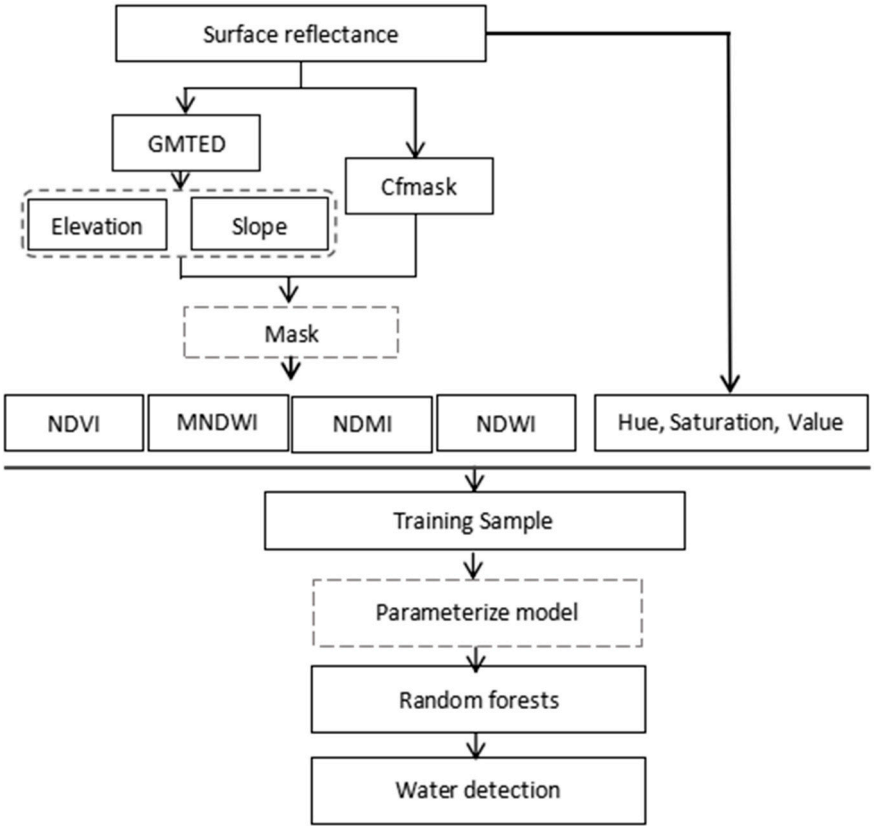

Figure 3. The flow chart of water classification.

2.9. Validation

The results of the classification were evaluated in terms of the errors of commission at the pixel scale. The validation design applied the validation method in Olofsson et al. (2014) [24] and took into account different sensors. The reference datasets were produced as follows. A random sample of 1416 pixels was generated from a region of interest. We applied 472 random points to the 2000, 2008, and 2016 water maps which represented Landsat 5, Landsat 7, and Landsat 8 results, respectively. Each map was classified into 3 classes: water (no change compared with 2000 water map), land (no change compared with 2000 water map), and the changing class. We applied the stratified sampling method for each map. Then, the properties of these points were determined by visual interpretation. The dataset was used to verify the classification of each year. Both the user's accuracy and the producer's accuracy were calculated. Table 1 shows the accuracy of the classification.

Table 1. The accuracy of classification.

Map		Reference			User's Accuracy
		Water	Land	Total	
Landsat5	Water	90	1	91	98.90%
	Land	17	364	381	95.54%
	Total	107	365	472	
	Producer's Accuracy	84.1%	99.7%		Total Accuracy: 96.19%
Landsat7	Water	88	2	90	97.8%
	Land	21	361	382	94.5%
	Total	109	363	472	
	Producer's Accuracy	80.7%	99.4%		Total Accuracy: 95.1%
Landsat8	Water	97	1	98	99.0%
	Land	15	359	374	96.0%
	Total	112	360	472	
	Producer's Accuracy	86.6%	99.7%		Total Accuracy: 96.6%

3. Results and Discussion

3.1. Results

Water detection was performed to collect 16 years' worth of data from 2000 to 2016. The data that was then used to investigate the surface water dynamics in the Arctic and boreal regions of North America. The distribution map of inland water is shown in Figure 4a. One can see that over the past 16 years, almost 3.2 km^2 of water disappeared, over 1.2 km^2 transitioned from land to water, and over 4.4 km^2 transitioned from water to land in the study area. Figure 4b shows an example of lake changes during the study period. Figures 5–7 shows the water dynamics in the entire region between 2000 and 2016. Figure 5 shows the trend of the dynamic in terms of the years. Figure 6 shows the trend of the dynamic by latitude and Figure 7 shows the trend of the dynamic by longitude. The loss of water indicates that the water in 2000 transformed into land in another year. Gain refers to the land in 2000 transforming into water in another year. Budget equals the amount of loss subtracted by the amount of gain. The percentage of the water area dynamics is an average of the total water bodies' dynamics from 2001 to 2016. In the statistical analysis, a 2° interval was set for the latitude and a 5° interval was set for the longitude.

From Figure 5, it seems that the water gain and loss shows a slowly increasing trend, with an exception in 2001. This means more and more water bodies are shrinking and expanding, or that more and more water appears and disappears. Such a finding may be related to the deepening active layer of permafrost [25] as well as the climatic factors [26]. The deepening active layer of permafrost can cause lateral erosion, which results in water body expansion and lateral drainage, and can also cause settlement at the lake bottom, which results in internal drainage. Even though the loss and gain areas increased, the budget did not change significantly as the emergence and disappearance areas of water are roughly equivalent. Thus, the Arctic does not appear to lose significant amounts of water. Additionally, surface water does not evaporate or drain underground much either. However, the budget trend is slightly decreasing, which implies that the water may decrease gradually in the future.

From Figure 6, the loss and gain areas rise abruptly at 70° N, where the coastal zone dominates, possibly due to the shrinking sea ice [27]. The shrinking sea ice results in higher temperatures and increased snowfall, which decreases the lake ice thickness. The budget dynamics of latitude shows a different pattern. The budget at 68° N begins to change abruptly and decreases as the latitude increases from 60° N to 68° N. The region above 68° N shows the same trend.

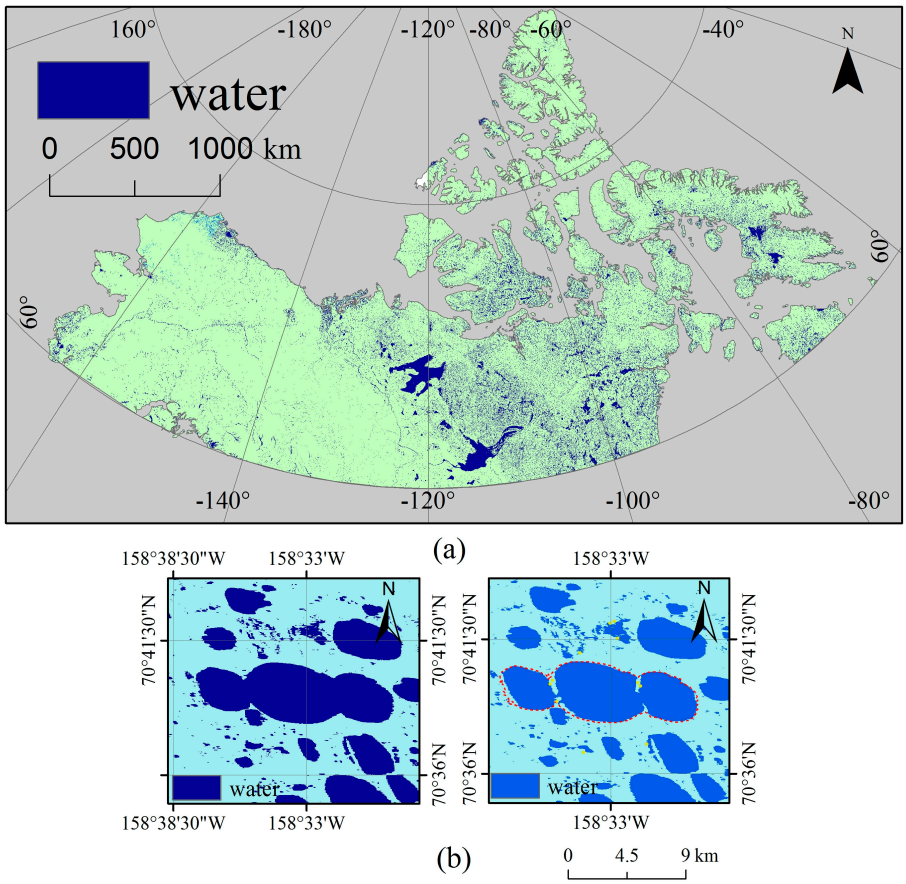

Figure 4. The maps showing (**a**) the distribution of inland water in the study area in 2016 and (**b**) a lake in the Barrow region in 2000 (**left**) and the lake in 2016 (**right**), showing a shrinkage over the 16-year period.

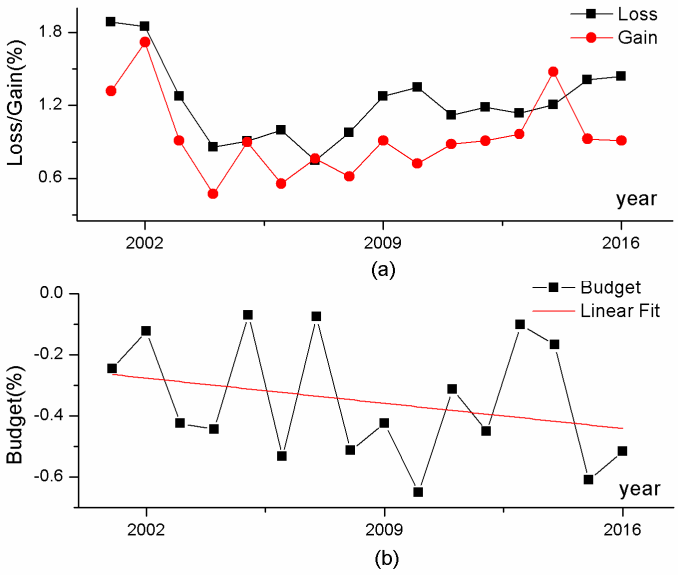

Figure 5. The dynamics of inland water over the years (the figure shows water dynamics per year across the study area), Figure (**a**) shows percentage of loss and gain area over the years and Figure (**b**) shows percentage of budget area over the years.

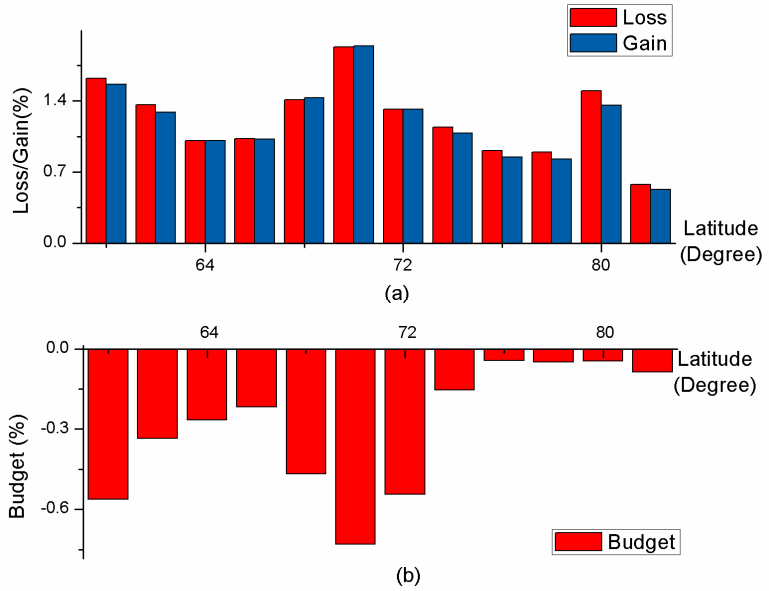

Figure 6. The dynamics of inland water according to the latitude (the figure showed the yearly average dynamics of water with latitude), the Figures (**a**) and (**b**) respectively repercent changing percentage of loss/gain and budget over the latitude.

From Figure 7, the water with longitude shows different dynamics—the loss and gain decrease more in the east than in the west. Moreover, budget in the east decreases more than in the west. The distribution with longitude may be related to the terrain, climate, and permafrost. Mountains in North America are distributed from 125° W to 160° W, which is different from the distribution pattern of the water longitude dynamics. Thus, the terrain does not impact the water dynamics significantly.

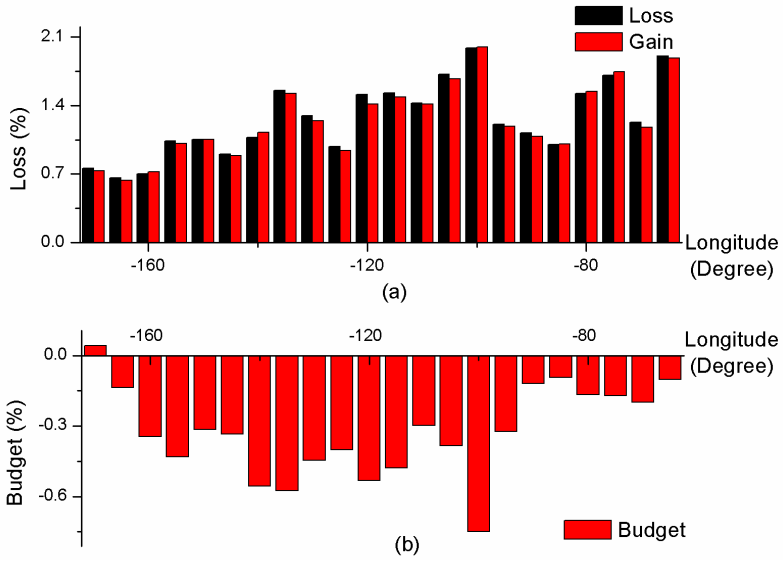

Figure 7. The dynamics of inland water according to the longitude (the figure shows the yearly average water dynamics with longitude), the Figures (**a**) and (**b**) respectively repercent changing percentage of loss/gain and budget over the longitude.

3.2. Discussion

Many studies on the trends of water and climate-driven effects on ponds have been conducted in the Arctic region. Some studies observed significant decreases in size and number, and some found

increases in the number, as well as in the area of lakes [9,28,29]. Obviously, the results are ambiguous and the reasons for the discrepancies are unclear. Site investigations suggest that permeability of soils, temperature, precipitation, shoreline erosion, and vegetation cover [1,4,30,31] may be related to these discrepancies, which need to be explored further.

We found that budget changes abruptly at 68° N (Figure 6) and changes more from 160° W to 100° W. This region is roughly consistent with the distribution of permafrost (Figure 8). We can further verify that the Arctic inland water dynamics are strongly correlated to permafrost [32–34]. In order to further confirm that the permafrost process impacts inland water dynamics, we calculated the loss, gain, budget area percentages from 2000 to 2016 with a 1° (latitude) × 5° (longitude) grid and calculated the correlation between the dynamic area and permafrost. We assigned the weight to the grid net based on the distribution of the permafrost. The weights of the continuous permafrost, the discontinuous permafrost, the sporadic permafrost, and the isolated permafrost were 0.95, 0.70, 0.30, and 0.05. The mean of the weight value within each grid was calculated. From Table 2, the loss and budget had a strong correlation with the distribution of the permafrost. The gain was unrelated to the permafrost weakly.

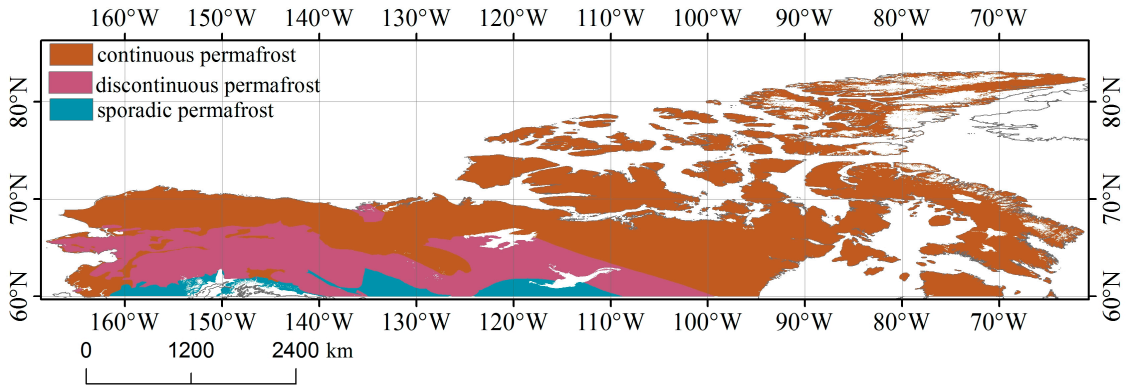

Figure 8. The permafrost map (permafrost data can be downloaded from the National Snow and Ice Data Center [35]).

Table 2. The correlation analysis.

Correlations	Gain	Loss	Budget
Spearman Correlations	0.35	0.62	−0.55
Kendall Correlations	0.25	0.49	−0.42

Permafrost thaw is related to the surface temperature. A different process of thaw occurs at different temperatures and, consequently, water will change at various levels. The paper uses the MODIS LST/Emissivity products, MYD11A2 and MOD11A2 [36,37], to analyze the water dynamics with annual average temperature differences (Figure 9). As observed in Figure 9, the paper found that the loss and gain of water showed the same trend. In the beginning, the loss and gain areas declined and then the loss and gain areas increased with the rising temperatures. However, this trend cannot be explained by temperature alone, as there are other factors (for example, Lake ice, wind, and morphological variables) involved in the process [34]. The budget shows a different trend—as the temperatures rise, the net loss increases at first and then decreases. This trend is consistent with the water response to permafrost thaw [26].

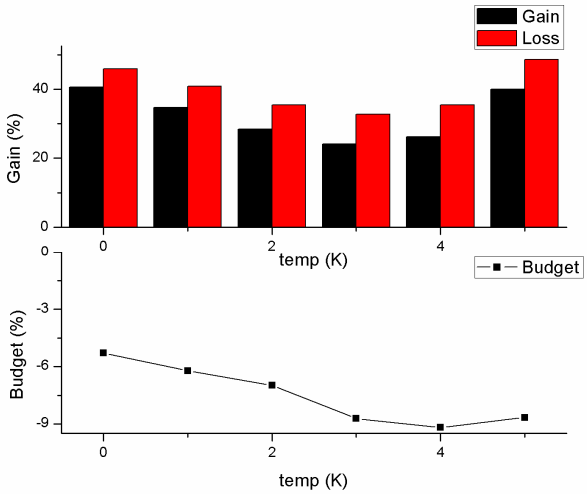

Figure 9. The dynamics of inland water according to the temperatures (the horizontal axis represents the yearly average temperature difference. The *x*-axis represents the daytime land surface temperature difference. The temperature difference is calculated with the mean temperature for the 16-year period, subtracting the mean temperature in 2000. The unit for the horizontal axis is Kelvin (K)).

4. Conclusions

The observations of surface water in the Arctic region show that the dynamics of surface water vary through time and space. These results help understand Arctic landscape dynamics. Many studies have analyzed the extent and amount of inland water using Landsat products of coarser or higher resolution. Some studies observed decreases, while some observed increases, and some found both. These changes become increasingly ambiguous with further research. As such, the controlling factors of these changes remain unclear. Accordingly, some studies investigated the factors from two perspectives: climatic factors and thermokarst processes. The present study investigated water dynamics at the continental scale and determined the spatial and temporal distribution using a high temporal resolution. The study also analyzed the reasons for these changes. The results showed that the water area is decreasing yearly in the long term, while water loss and gain always show similar dynamic patterns both latitudinally and longitudinally with the loss of water and the gain of water roughly offsetting one another. In addition, the spatial distribution of the water budget is strongly linked to permafrost—it seems that permafrost determines the distribution pattern of the water dynamics more than climatic factors (for example, temperature). Moreover, in continuous permafrost regions, the water net loss decreases as the latitude increases. The same pattern was present in the discontinuous permafrost and sporadic permafrost regions. Loss and gain water show the same pattern with surface temperature, but the pattern of the dynamics cannot be explained by temperature alone. The budget presents a pattern with the surface temperature, which can be explained by the fact that temperature affects permafrost thaw.

Author Contributions: Y.S. designed and performed the experiments and wrote the manuscript. F.S. helped to analyze the data and made significant suggestions to the text. D.F. implemented the code, ensured successful runs, and contributed to the data collection and the text with comments and suggestions. W.X. completed the diagrams and maps and provided suggestions to the text.

Funding: The work was supported by the National Key R&D Program of China (2016YFC1402701). This research was also supported by the Youth Science Funds of State Key Laboratory of Resources and Environmental Information System (O8R8A080YA), Chinese Academy of Sciences, and the research grants (Y6V60206YZ) funded by Institute of Geographic Sciences and Natural Resources Research, Chinese Academy of Sciences.

Acknowledgments: The authors thank other colleagues and friends in the field for their help and suggestions.

Conflicts of Interest: The authors declare no conflict of interest.

References

1. Riordan, B.; Verbyla, D.; McGuire, A.D. Shrinking ponds in subarctic Alaska based on 1950–2002 remotely sensed images. *J. Geophys. Res. Biogeosci.* **2006**, *111*. [CrossRef]
2. Smith, A.R. Color gamut transform pairs. *ACM Siggraph Comput. Graph.* **1978**, *12*, 12–19. [CrossRef]
3. Smith, L.C.; Sheng, Y.; MacDonald, G.M.; Hinzman, L.D. Disappearing Arctic lakes. *Science* **2005**, *308*, 1429. [CrossRef] [PubMed]
4. Jones, B.M.; Grosse, G.; Arp, C.D.; Jones, M.C.; Walter, K.M.; Anthony, V.E. Romanovsky Modern thermokarst lake dynamics in the continuous permafrost zone, northern Seward Peninsula, Alaska. *J. Geophys. Res. Biogeosci.* **2011**, *116*. [CrossRef]
5. Carroll, M.L.; Loboda, T.V. Multi-Decadal Surface Water Dynamics in North American Tundra. *Remote Sens.* **2017**, *9*, 497. [CrossRef]
6. MacDonald, G.M. Water, climate change, and sustainability in the southwest. *Proc. Natl. Acad. Sci. USA* **2010**, *107*, 21256–21262. [CrossRef] [PubMed]
7. Prigent, C.; Papa, F.; Aires, F.; Jimenez, C.; Rossow, W.B.; Matthews, E. Changes in land surface water dynamics since the 1990s and relation to population pressure. *Geophys. Res. Lett.* **2012**, *39*. [CrossRef]
8. Tulbure, M.G.; Broich, M.; Stehman, S.V.; Kommareddy, A. Surface water extent dynamics from three decades of seasonally continuous Landsat time series at subcontinental scale in a semi-arid region. *Remote Sens. Environ.* **2016**, *178*, 142–157. [CrossRef]
9. Nitze, I.; Grosse, G.; Jones, B.M. Landsat-based trend analysis of lake dynamics across northern permafrost regions. *Remote Sens.* **2017**, *9*, 640. [CrossRef]
10. Feng, M.; Sexton, J.O.; Channan, S.; Townshend, J.R. A global, high-resolution (30-m) inland water body dataset for 2000: First results of a topographic–spectral classification algorithm. *Int. J. Digit. Earth* **2016**, *9*, 113–133. [CrossRef]
11. Donchyts, G.; Baart, F.; Winsemius, H.; Gorelick, N.; Kwadijk, J.; van de Giesen, N. Earth's surface water change over the past 30 years. *Nat. Clim. Chang.* **2016**, *6*, 810–813. [CrossRef]
12. Carroll, M.; Wooten, M.; DiMiceli, C.; Sohlberg, R.; Kelly, M. Quantifying Surface Water Dynamics at 30 Meter Spatial Resolution in the North American High Northern Latitudes 1991–2011. *Remote Sens.* **2016**, *8*, 622. [CrossRef]
13. Pekel, J.F.; Cottam, A.; Gorelick, N.; Belward, A.S. High-resolution mapping of global surface water and its long-term changes. *Nature* **2016**, *540*, 418–422. [CrossRef] [PubMed]
14. Paltan, H.; Dash, J.; Edwards, M. A refined mapping of Arctic lakes using Landsat imagery. *Int. J. Remote Sens.* **2015**, *36*, 5970–5982. [CrossRef]
15. Eros Science Processing Architecture. Available online: https://espa.cr.usgs.gov/ (accessed on 24 July 2016).
16. Gao, B.C. NDWI—A normalized difference water index for remote sensing of vegetation liquid water from space. *Remote Sens. Environ.* **1996**, *58*, 257–266. [CrossRef]
17. Tucker, C.J.; Pinzon, J.E.; Brown, M.E.; Slayback, D.A.; Pak, E.W.; Mahoney, R.; Vermote, E.F.; El Saleous, N. An extended AVHRR 8-km NDVI dataset compatible with MODIS and SPOT vegetation NDVI data. *Int. J. Remote Sens.* **2005**, *26*, 4485–4498. [CrossRef]
18. Wilson, E.H.; Sader, S.A. Detection of forest harvest type using multiple dates of Landsat TM imagery. *Remote Sens. Environ.* **2002**, *80*, 385–396. [CrossRef]
19. Xu, H. Modification of normalised difference water index (NDWI) to enhance open water features in remotely sensed imagery. *Int. J. Remote Sens.* **2006**, *27*, 3025–3033. [CrossRef]
20. Danielson, J.J.; Gesch, D.B. *Global Multi-Resolution Terrain Elevation Data 2010 (GMTED2010)*; USGS Report 2011-1073; US Geological Survey: Reston, VA, USA, 2011. Available online: https://pubs.er.usgs.gov/publication/ofr20111073 (accessed on 20 July 2016).
21. Arendt, A.; Bliss, A.; Bolch, T.; Cogley, J.G.; Gardner, A.S.; Hagen, J.-O.; Hock, R.; Huss, M.; Kaser, G.; Kienholz, C.; et al. *Randolph Glacier Inventory—A Dataset of Global Glacier Outlines: Version 5.0*; Global Land Ice Measurements from Space; Digital Media: Boulder, CO, USA, 2015. Available online: http://www.glims.org/RGI/ (accessed on 20 July 2016).
22. Carroll, M.L.; Townshend, J.R.; DiMiceli, C.M.; Noojipady, P.; Sohlberg, R.A. A new global raster water mask at 250 m resolution. *Int. J. Digit. Earth* **2009**, *2*, 291–308. [CrossRef]
23. Breiman, L. Random forests. *Mach. Learn.* **2001**, *45*, 5–32. [CrossRef]

24. Olofsson, P.; Foody, G.M.; Herold, M.; Stehman, S.V.; Woodcock, C.E.; Wulder, M.A. Good practices for estimating area and assessing accuracy of land change. *Remote Sens. Environ.* **2014**, *148*, 42–57. [CrossRef]
25. Jorgenson, M.T.; Romanovsky, V.; Harden, J.; Shur, Y.; O'Donnell, J.; Schuur, E.A.G.; Kanevskiy, M.; Marchenko, S. Resilience and vulnerability of permafrost to climate change. *Can. J. For. Res.* **2010**, *40*, 1219–1236. [CrossRef]
26. Karlsson, J.M.; Jaramillo, F.; Destouni, G. Hydro-climatic and lake change patterns in Arctic permafrost and non-permafrost areas. *J. Hydrol.* **2015**, *529*, 134–145. [CrossRef]
27. Brock, B.W. Shrinking sea ice, increasing snowfall and thinning lake ice: A complex Arctic linkage explained. *Environ. Res. Lett.* **2016**, *11*, 091004. [CrossRef]
28. Koch, J.C. Lateral and subsurface flows impact Arctic coastal plain lake water budgets. *Hydrol. Process.* **2016**, *30*, 3918–3931. [CrossRef]
29. Carroll, M.L.; Townshend, J.R.G.; DiMiceli, C.M.; Loboda, T.; Sohlberg, R.A. Shrinking lakes of the Arctic: Spatial relationships and trajectory of change. *Geophys. Res. Lett.* **2011**, *38*. [CrossRef]
30. Jepsen, S.M.; Voss, C.I.; Walvoord, M.A.; Minsley, B.J.; Rover, J. Linkages between lake shrinkage/expansion and sublacustrine permafrost distribution determined from remote sensing of interior Alaska, USA. *Geophys. Res. Lett.* **2013**, *40*, 882–887. [CrossRef]
31. Roach, J.; Griffith, B.; Verbyla, D.; Jones, J.B. Mechanisms influencing changes in lake area in Alaskan boreal forest. *Glob. Chang. Biol.* **2011**, *17*, 2567–2583. [CrossRef]
32. Karlsson, J.M.; Lyon, S.W.; Destouni, G. Thermokarst lake, hydrological flow and water balance indicators of permafrost change in Western Siberia. *J. Hydrol.* **2012**, *464*, 459–466. [CrossRef]
33. Van Huissteden, J.; Berrittella, C.; Parmentier, F.J.W.; Mi, Y.; Maximov, T.C.; Dolman, A.J. Methane emissions from permafrost thaw lakes limited by lake drainage. *Nat. Clim. Chang.* **2011**, *1*, 119–123. [CrossRef]
34. Šmejkalová, T.; Edwards, M.E.; Dash, J. Arctic lakes show strong decadal trend in earlier spring ice-out. *Sci. Rep.* **2016**, *6*, 38449. [CrossRef] [PubMed]
35. Brown, J.; Ferrians, J.O., Jr.; Heginbottom, J.A.; Melnikov, E.S. *Circum-Arctic Map of Permafrost and Ground-Ice Conditions*; Version 2; National Snow and Ice Data Center: Boulder, CO, USA, 2002.
36. Wan, Z.; Hook, S.; Hulley, G. *MOD11A2: MODIS/Terra Land Surface Temperature/Emissivity 8-Day L3 Global 1 km SIN Grid*; NASA EOSDIS Land Processes DAAC; USGS Earth Resources Observation and Science (EROS) Center: Sioux Falls, SD, USA. Available online: https://lpdaac.usgs.gov (accessed on 16 June 2016).
37. Wan, Z.; Hook, S. *MYD11A2: MODIS/Aqua Land Surface Temperature/Emissivity 8-Day L3 Global 1 km SIN Grid*; V006. NASA EOSDIS Land Processes DAAC; USGS Earth Resources Observation and Science (EROS) Center: Sioux Falls, SD, USA. Available online: https://lpdaac.usgs.gov (accessed on 17 July 2014).